Wind and Structures, *Vol. 17, No. 3(2013) 317-343*
DOI:http://dx.doi.org/10.12989/was.2013.17.3.317

Yaw wind effect on flutter instability of four typical bridge decks

Le-Dong Zhu[*1,2,3,4], You-Lin Xu[2], Zhenshan Guo[3,4], Guang-Zhao Chang[5] and Xiao Tan[5]

[1]*State Key Laboratory for Disaster Reduction in Civil Engineering, Tongji University, Shanghai 200092, China*
[2]*Department of Civil and Environmental Engineering, The Hong Kong Polytechnic University, Hung Hom, Kowloon, Hong Kong, China*
[3]*Key Laboratory of Wind Resistance Technology of Bridges (Shanghai) of Ministry of Transport, Tongji University, Shanghai 200092, China*
[4]*Department of Bridge Engineering, Tongji University, Shanghai 200092, China*
[5]*Lin Tung-Yen and Li Guo-Hao Consultants LTD, Shanghai 200437, China*

(Received August 9, 2012, Revised January 25, 2013, Accepted March 30, 2013)

Abstract. When evaluating flutter instability, it is often assumed that incident wind is normal to the longitudinal axis of a bridge and the flutter critical wind speed estimated from this direction is most unfavorable. However, the results obtained in this study via oblique sectional model tests of four typical types of bridge decks show that the lowest flutter critical wind speeds often occur in the yaw wind cases. The four types of bridge decks tested include a flat single-box deck, a flat π-shaped thin-wall deck, a flat twin side-girder deck, and a truss-stiffened deck with and without a narrow central gap. The yaw wind effect could reduce the critical wind speed by about 6%, 2%, 8%, 7%, respectively, for the above four types of decks within a wind inclination angle range between -3° and 3°, and the yaw wind angles corresponding to the minimal critical wind speeds are between 4° and 15°. It was also found that the flutter critical wind speed varies in an undulate manner with the increase of yaw angle, and the variation pattern is largely dependent on both deck shape and wind inclination angle. Therefore, the cosine rule based on the mean wind decomposition is generally inapplicable to the estimation of flutter critical wind speed of long-span bridges under skew winds. The unfavorable effect of yaw wind on the flutter instability of long-span bridges should be taken into consideration seriously in the future practice, especially for supper-long span bridges in strong wind regions.

Keywords: long-span bridge; flutter; yaw wind effect; flat single-box deck; flat π-shaped thin-wall deck; flat twin side-girder deck; truss-stiffened deck

1. Introduction

As a most dangerous wind-induced instability phenomenon, flutter of a long-span bridge must be avoided. When evaluating flutter instability of a long-span bridge, it is often assumed that wind direction normal to the bridge span is a most unfavorable case. Therefore, the coming winds are commonly regarded to be normal to the bridge span in the traditional analyses for flutter instability and control, although many complex factors, such as the effects of aerodynamic coupling, multi-

*Corresponding author, Professor, E-mail: ledong@tongji.edu.cn

http://www.techno-press.org/?journal=was&subpage=8 ISSN: 1226-6116 (Print), 1598-6225 (Online)

mode coupling, full-order flutter, lateral-motion-correlative flutter derivatives, non-linear wind-induced large static deformations and wind turbulence, etc., are included in the analyses on the other hand (Scanlan and Gade 1977, Scanlan 1978, Agar 1989, Namini 1992, Jain *et al*. 1996, Katsuchi 1999, Ge and Tanaka 2000, Ding *et al*. 2002, Zhang and Brownjohn 2005, Zahlten and Eusani 2006, Chen 2007, Zhang 2007, Mishra *et al*. 2008a,b, Hua and Chen 2008, Zhang *et al*. 2010, Øiseth *et al*. 2011, Phan *et al*. 2011, Zhang *et al*. 2011, Kirch and Peil 2011). However, strong winds at a given bridge site seldom attack the bridge at a right angle to the longitudinal axis of the bridge span but generally at certain yaw angles instead as observed from field measurements (Bietry 1994, Xu *et al*. 2000, Xu and Zhu 2005). For yaw wind cases, simple approaches based on mean wind decomposition are conventionally used in the estimations of buffeting responses (Xie and Tanaka 1991, Kimura and Tanaka 1992, Scanlan 1993, Kimura *et al*. 1994, Strømmen and Hjorth-Hasen 1995, Kimura and Ohara 1999). The mean wind is first decomposed into a cosine component normal to the bridge span and a sine component parallel to the bridge span, and the latter is then ignored. This decomposition approach is hence simply called "cosine rule". The traditional concept of mean wind decomposition is also employed sometimes for estimating the flutter critical wind speed under yaw wind condition. This means that a given yaw wind speed is assumed to be critical for flutter if its cosine component equals the critical wind speed in normal wind case.

In 1999, Scanlan proposed an approximate skew wind theory for estimating flutter critical wind speeds of bridges under skew (both yawed and inclined) winds (Scanlan 1999). In this theory, the aeroelastic performance of an oblique cross-section in the mean wind direction is supposed to be similar to that of the true cross-section normal to the bridge span when the yaw wind angle is not large and the bridge deck is rather flat. In light of this assumption, a relationship between the aerodynamic derivative A_2^* of the oblique cross-section and that of the true cross-section can be established, and the flutter critical wind speed under skew wind can be estimated according to the single DOF torsional flutter theory. However, for bridges with flat bridge decks, the flutter pattern often shows a manner of coupled vertical-torsional vibration, and the value of A_2^* may never become positive. Furthermore, if a bridge deck is of an open cross-section with transverse diaphragms exposed to wind, the aeroelastic behavior of an oblique cross-section may be significantly different from that of the true cross-section. The Scanlan's skew wind theory may not be adequate to address these cases.

According to the cosine role, the flutter critical wind speed increases with the increase of yaw angle. Nevertheless, the researches on the flutter instability and buffeting responses of the Tsing Ma Bridge under skew wind, carried out by the 1st and 2nd authors and their co-workers (Zhu *et al*. 2002a, Zhu *et al*. 2005), showed that the yaw wind effect may have unfavorable effects on both flutter critical wind speed and buffeting response. Since the Tsing Ma bridge deck has a bluff-box cross-section with a small width-to-height ratio of only 5.37 and one central vent slot on each of its upper and lower layers (Zhu *et al*. 2002b), one may concern yaw wind effects on various flat decks because these decks are typical types of bridge decks frequently used in the practice. Moreover, the yaw wind effect on the flutter instability of truss-stiffened deck bridges is also interesting to know as truss-stiffened decks are prevailing as well in the practice of bridge engineering. Hence, the yaw wind effect on the flutter instabilities of the above-mentioned four typical types of bridge decks were investigated in this study by means of oblique sectional model tests in a wind tunnel, and the results are analyzed and presented in the following sections.

2. Description of bridge types

2.1 Bridge with a flat single-box deck

Flat single-box deck is one of the most commonly used decks in long-span cable-supported bridges. To study the yaw wind effect on the flutter instability of this type of bridge deck, the 3rd Nanjing Bridge over Yangtze River in Jiangsu Province (see Fig. 1) is taken as an example in this study. The bridge, open to the public in October 2005, is a cable-stayed bridge with five spans of 63+257+648 +257+63 m and an inclined cable system. It has a steel deck with flat single-box cross-section of 3.2 m in height and 37.16 m in width (see Fig. 2). The width-to-height ratio of the deck is about 11.61. Its two 220m high towers are of frame-structure and each of them is compounded of a major steel part over the bridge deck (179.25 m) and a concrete part below the bridge deck (35.75 m). The fundamental vertical and torsional natural frequencies obtained via the finite element analysis with ANSYS are 0.2348 Hz and 0.6205 Hz, respectively. The torsional-vertical frequency ratio is thus about 2.64. The corresponding equivalent mass (m_{eq}) and equivalent mass moment of inertia (I_{meq}) of the bridge deck considering the effect of whole bridge 3D vibration are 2.57×104 kg/m and 2.63×106 kgm2/m, respectively (Zhu and Xiang 1995).

Fig. 1 The 3rd Nanjing Bridge over Yangtze River

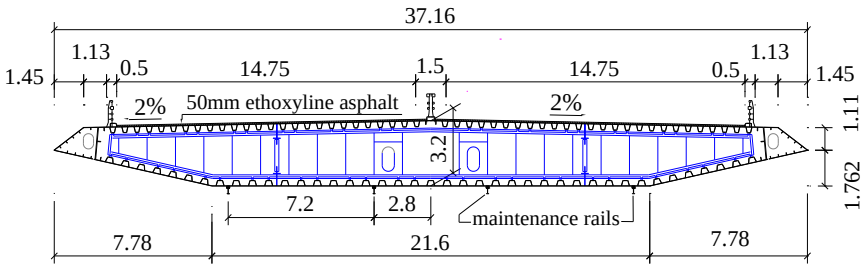

Fig. 2 Deck cross-section of the 3rd Nanjing Bridge over Yangtze River

2.2 Bridge with a flat π-shaped thin-wall deck

Flat π-shaped thin-wall deck is also a common deck type of long-span cable-supported bridges. In this study, the Hongguang Bridge over Liu River (see Fig. 3) in Liuzhou, Guangxi Zhuangzu Autonomous Region, is taken as another example to investigate the yaw wind effect on the flutter instability of this kind of bridge deck. This bridge, open to the public in August 2004, is a single-span suspension bridge with a steel deck of flat π-shaped thin-wall cross-section, which is 2.2 m in height and 27.6 m in width (see Fig. 4). The width-to-height ratio of the deck is equal to 12.55. Its span length is 380 m, and two RC arch-frame bridge towers are 76 m high. The sag-to-span ratio of the main cables is 1/9.87. The fundamental vertical and torsional natural frequencies obtained via the finite element analysis are 0.2768 Hz and 0.3744 Hz. The torsional-vertical frequency ratio is about 1.35. The corresponding equivalent mass (m_{eq}) and equivalent mass moment of inertia (I_{meq}) of the bridge deck are 1.5868×104kg/m and 1.2206×106 kgm2/m, respectively. Furthermore, a 0.7 m-high skirt plate was mounted at each of the two edges of the π-shaped deck to improve the flutter critical wind speed of the bridge.

Fig. 3 Hongguang Bridge over Liu River in Liuzhou

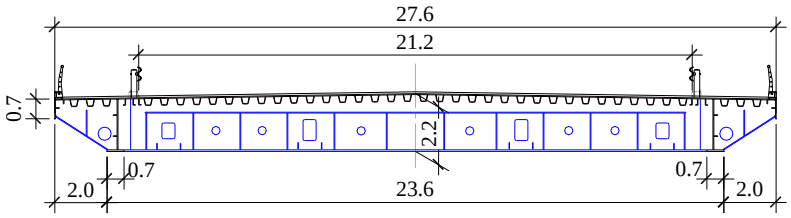

Fig. 4 Deck cross-section of the Hongguang Bridge over Liu River

2.3 Bridge with a flat twin side-girder deck

Flat twin side-girder deck is frequently used in long-span PC cable-stayed bridges in China.

The 2nd Chongqing Bridge over Yangtze River (also called Lijiatuo Bridge) in Chongqing Municipality, as shown in Fig. 5, is a typical and early one of this kind of bridges. It is thus taken as an engineering background in this study to investigate the flutter instability of flat twin side-girder decks under yaw wind condition. This bridge was finished at the end of 1996, and has a main span of 444 m, two side spans of 169 m and two transition spans of 53 m. Its two bridge towers of H-style are 137 in height with 111 m above the bridge deck. As shown in Fig. 6, the bridge deck is 24 m wide and 2.6 m high, and with two side-girders of 1.7 m in width and 2.5 m in height. The width-to-height ratio of the deck is equal to 9.23. The fundamental vertical and torsional natural frequencies obtained via the finite element analysis are 0.2872 Hz and 0.4619 Hz.

The torsional-vertical frequency ratio is about 1.61. The corresponding equivalent mass (m_{eq}) and equivalent mass moment of inertia (I_{meq}) of the bridge deck are 5.1132×104 kg/m and 3.0134×106 kgm2/m, respectively.

Fig. 5 The 2nd Chongqing Bridge over Yangtze River

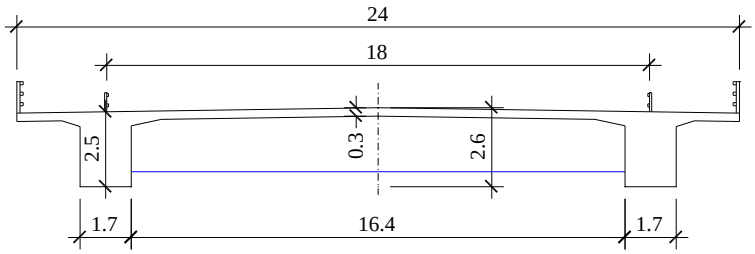

Fig. 6 Deck cross-section of the 2nd Chongqing Bridge over Yangtze River

2.4 Bridge with a truss-stiffened deck

Truss-stiffened deck bridges are very popular in USA and Japan, and they now become more and more prevailing in the mountain regions of the west China. In this study, Balinghe Bridge, located in the south-west part of Guizhou Province in China, is selected as a background for the investigation on the flutter instability of truss-stiffened decks under yaw wind condition. This bridge, open to the public in December 2009, is a long-span suspension bridge with a 1088 m-span

truss-stiffened deck (see Fig. 7), crossing the Balinghe deep gorge of about 560 m in depth at a 368m level (about 2/3 depth) above the gorge bottom, which is 680m in altitude. The altitudes of the whole bridge are between 956.000 m and 1160.516 m. For more details about the gorge of Balinghe, one can refer to the literature (Zhu *et al*. 2011).

Fig. 7 Balinghe Bridge over the deep gorge of Baling River

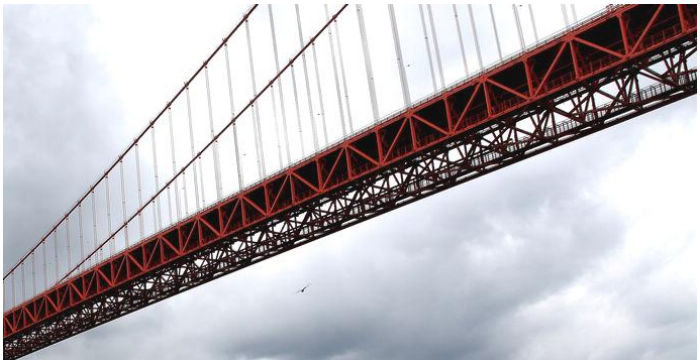

(a) Truss pattern

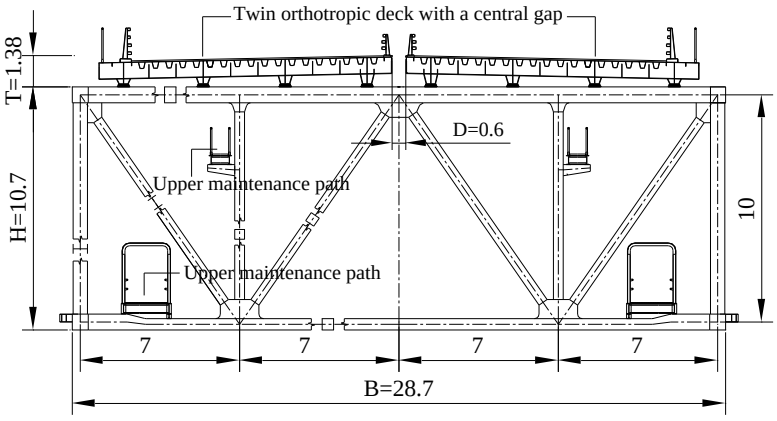

(b) Cross section

Fig. 8 Truss-stiffened girder and deck of Balinghe Bridge (unit: mm)

As shown in Fig. 8, the stiffening spatial truss girder is comprised of two vertical main trusses, a series of transverse trusses, one top horizontal brace system and one bottom horizontal brace system. The vertical main truss is composed of an upper chord, a lower chord, a series of vertical and batter webs. The central distance between the two main trusses is 28.0 m, and the central distance between the upper and lower chords of the main truss is 10.0 m. The overall height of the stiffening truss girder is 10.7 m and its overall width is 28.7 m. The length of a standard truss segment is 10.8 m. Closed square-box cross-sections are used for the upper and lower chords, the batter webs of the main trusses, whilst a H-shaped cross-section is used for the most of the vertical webs. Each transverse truss is comprised of a pair of upper and lower transverse beams, a pair of vertical webs, a pair of inboard oblique webs and a pair of outboard oblique webs. The outboard webs of the transverse truss have a H-shaped cross-section whilst the other members possess closed square-box cross-sections. Both the top and bottom horizontal brace systems are of K-shaped pattern, and closed square-box cross-sections are chosen for their members.

As shown in Fig. 8(b), twin separate decks of orthotropic steel plates with a central gap of 0.6 m are adopted in this bridge. The orthotropic decks are comprised of steel plates, longitudinal U-shaped and plate-shaped stiffening ribs, transverse beams, and longitudinal inverse T-shaped beams which are connected to the upper transverse beams of the transverse trusses using pull-press-resistant basin-type rubber bearers. The overall height of the single orthotropic deck is 1.38 m and its width 12.90 m.

The natural frequencies of the first vertical and torsional symmetric modes obtained via the finite element analysis with ANSYS are 0.1545 Hz and 0.2780 Hz, respectively. The torsional-vertical frequency ratio is thus about 1.8. The corresponding equivalent mass (m_{eq}) and equivalent mass moment of inertia (I_{meq}) of the truss-stiffened deck are 2.9623×10^4 kg/m and 4.7045×10^6 kgm^2/m, respectively.

3. Configurations and tests of oblique sectional models

The wind tunnel tests of spring-suspended oblique sectional models were carried out in the TJ-2 Wind Tunnel of the State Key Laboratory for Disaster Reduction in Civil Engineering at Tongji University, China, for all the four bridges mentioned before. The TJ-2 Wind Tunnel is a boundary layer wind tunnel of closed-circuit-type. The working section of the tunnel is 3 m wide, 2.5 m high and 15 m long. The achievable mean wind speed ranges from 0.5 m/s to 68.0 m/s, adjustable continuously. Both the vertical inclination angle of wind flow deviating from the horizontal plane and the horizontal yaw angle of wind flow deviating from the longitudinal symmetric axis of the wind tunnel are smaller than 0.5°.

As shown in Fig. 9, the inclination angle (θ) of wind in this study is defined as the angle between the mean wind and the deck plane, and the yaw angle (β) of wind is defined as the angle between the vertical plane through the mean wind vector and the vertical plane normal to the bridge span. The plane configuration of the oblique sectional models is shown in Fig. 10. Each oblique sectional model has a parallelogram plane, and is comprised of one rectangular middle segment with the length of L_c and two trapezoidal end parts with the average length of $(L\text{-}L_c)/2$, where L is the total axial length of the oblique sectional model. The function of the two trapezoidal end parts is to adjust the shapes of the whole oblique model ends to ensure that the two ends are always parallel to the mean wind direction during the test, so that the unfavorable effect of the 3D flows near the two model ends on the test results can be minimized. Therefore, different end parts

should be used in the tests for different yaw angles of wind (β), and the end parts should be removable. However, the lengths of the middle part (L_c) and the whole model (L) remain unchanged during the test for all yaw angles of wind. In the normal wind case (i.e., β=0°), the two end parts become rectangular.

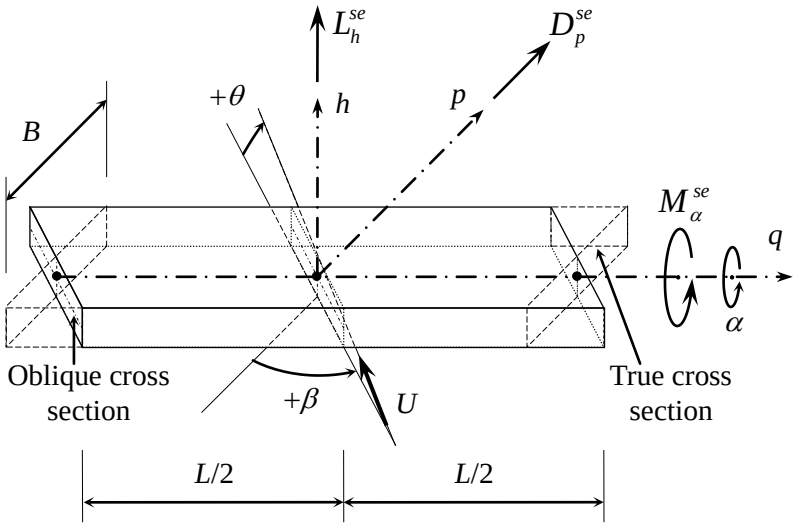

Fig. 9 Schematic diagram for the definitions of yaw and inclination angles of wind

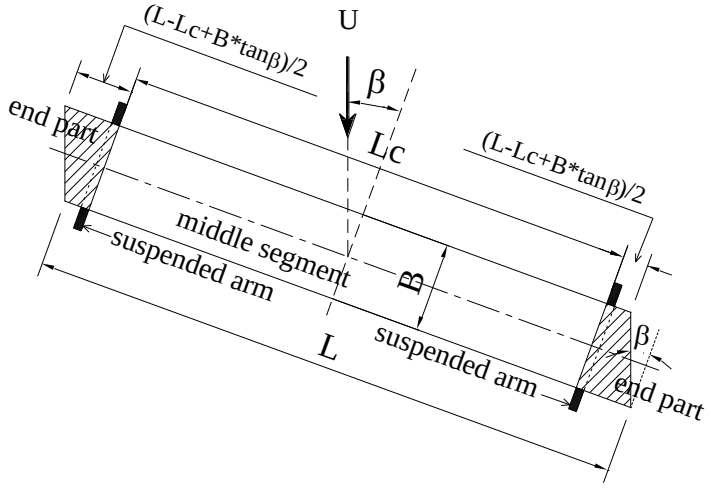

Fig. 10 Schematic diagram for the configuration of oblique sectional model

In the conventional sectional model test under a normal wind, two end plates with a size properly larger than the deck cross section are often attached at both ends of the model to eliminate the 3D flows around the model ends, which are mainly caused by the unbalance of the pressures between the upper and lower sides of the deck. However, in the yaw wind cases, there are some

span-wise flow components produced due to the guidance of the model front surface and the model top or bottom surface when the wind inclination angle is negative or positive. Therefore, the end plates have to be discarded in the yaw wind cases to avoid obstructing the span-wise flows. In this connection, the length-to-width ratio (*L/B*) of the oblique sectional model should be as large as possible to reduce the effect of 3D flows around the two model ends on the test results. It is generally suggested that *L/B* should be not less than 5. Further details on the test set-up of oblique sectional models can be found in the literature (Zhu *et al*. 2002b).

In this study, the geometric length scales of the four oblique sectional models were 1/90, 1/60, 1/70 and 1/60, respectively, for the 3rd Nanjing Bridge over Yangtze River with a flat single-box deck, the Liuzhou Hongguang Bridge with a flat π-shaped thin-wall deck, the 2nd Chongqing Bridge over Yangtze River with a flat twin side-girder deck, and the Balinghe Bridge with truss-stiffened deck. The lengths of the four models were, 2.814 m, 2.666 m, 2.683 m and 2.744 m, respectively, and the length-to-width ratios (*L/B*) of the four models were 6.81, 5.76, 7.82 and 5.74, respectively.

In the tests, the oblique sectional models were suspended in the wind tunnel with eight helical springs from the four steel tracks mounted on the ceiling and floor, as shown in Fig. 11. The two transverse suspended arms were, respectively, through the two end parts of the sectional model and were connected to the metal end plates (for non-truss-stiffened decks) or frames (for truss-stiffened deck) of the middle part of the sectional model. They were kept horizontal for all the inclination angles and yaw angles of wind by adjusting elaborately the length of the 8 turnbuckle screws connected to the springs.

(a) Twin side-girder deck (b)Truss-stiffened deck

Fig. 11 The oblique sectional model suspended in TJ-2 Wind Tunnel

The anticipated yaw angle (β) can be easily attained by fitting the 8 turnbuckle screws connected to the helical springs at proper locations on the tracks, whilst the desired inclination angle can be achieved by rotating the deck model around the central axis trough the centers of the two suspended arms, and fixed by inserting the bolts into the corresponding positioning holes preset on both the model end plates or frames and the suspended arms. However, one may notice the slight difference between the actual inclination angle (θ) and the rotation angle of the model (θ_m). Corresponding to the different model rotation angles, the actual wind inclination angle can be determined by the following equation and listed in Table 1:

$$\theta = \theta_m \cos\beta \tag{1}$$

Furthermore, to prevent the model from any significant lateral (or along-wind) static and dynamic displacements, it was restrained with four long tight metal wires with small springs in along-wind direction.

Table 1 Wind inclination angles corresponding to different model rotation angles

θ_m \ β	-5°	-3°	0°	3°	5°
0°	-5°	-3°	0°	3°	5°
5°	-4.98°	-2.99°	0°	2.99°	4.98°
10°	-4.92°	-2.95°	0°	2.95°	4.92°
15°	-4.83°	-2.90°	0°	2.90°	4.83°
20°	-4.70°	-2.82°	0°	2.82°	4.70°
30°	-4.33°	-2.60°	0°	2.60°	4.33°

4. Test results of flutter critical wind speeds

The flutter critical wind speeds of the above-mentioned four types of bridge decks were tested under skew wind condition with various combinations of wind yaw and inclination angles by using the approach of vertical-torsional coupled vibration stimulated by initial excitation. The vertical and torsional vibration damping ratios of the oblique sectional model system were identified at first for all concerned wind directions and all testing wind speeds. Normally, with the increase of wind speed, the damping ratios of torsional vibration increased first and then dropped towards zero or negative, whilst the damping ratio of vertical vibration increased all the way through. The flutter critical wind speeds were then obtained based on the gained variation curves of torsional damping ratio vs. testing wind speed according to the criteria of zero system damping. The corresponding velocity scales were about 1/10.55, 1/5.54, 1/4.94, and 1/5.00, respectively, for the flat single-box deck, the flat π-shaped thin-wall deck, the flat twin side-girder deck, and the truss-stiffened deck, and could slightly vary with the possible small change of the model frequencies due to the variation of model posture for different wind directions. The test results are analyzed and discussed below.

A total of 30 different wind directions which consist of six wind yaw angles (β) of 0°, 5°, 10°, 15°, 20°, 30° and five model rotation angles (θ_m) of ±5°, ±3°, 0° were considered in the skew wind flutter tests of the flat single-box deck, the flat π-shaped thin-wall deck and the flat twin side-girder deck, whilst only 12 wind directions which are composed of four wind yaw angles (β) of 0°, 5°, 10°, 15° and three model rotation angles (θ_m) of ±3°, 0° were taken into account in the skew wind flutter test of the truss-stiffened deck. The flutter critical wind speeds at various integer wind inclination angles provided thereinafter were calculated via the spline interpolation or extrapolation approaches based on the critical wind speed data directly obtained from the tests at the testing wind inclination angles shown in Table 1, which correspond to the integer model rotation angles.

4.1 Flat single-box deck

The structural damping ratio of the sectional model system of the flat single-box deck was about 0.5% for all the test cases and varied somewhat with the change of the model posture. Fig. 12 shows the spline-fitted curves of the torsional vibration damping ratios of the flat single-box deck model system vs. the test wind speed for different wind yaw angles and different model rotation angles, where the structural damping ratio of the model system at the zero wind speed was corrected to 0.5% for all test cases. The flutter critical wind speeds of the sectional model system corresponding to various wind yaw angles and model rotational angles can then be determined by finding the zero-damping points according to these spline-fitted curves. The flutter critical wind speeds at various integer inclination angles can be calculated via the spline interpolations for each wind yaw angle.

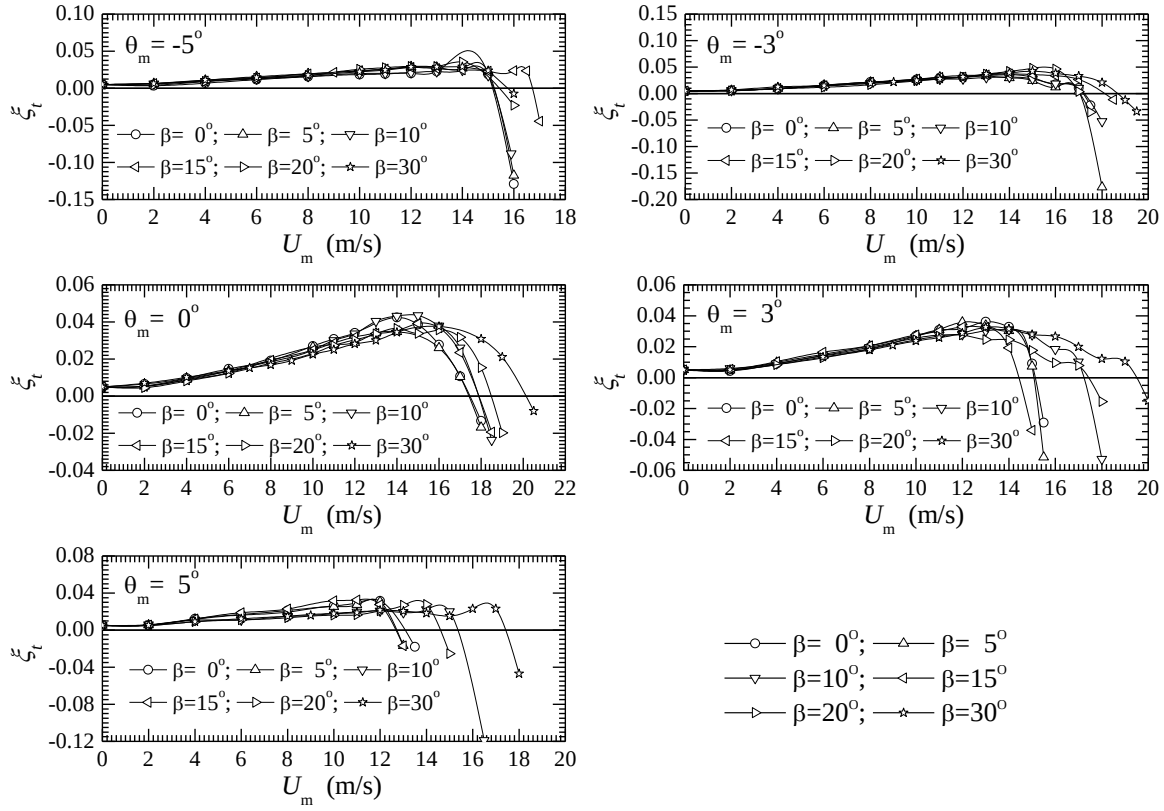

Fig.12 Torsional vibration damping ratios of the flat single-box deck model vs. wind speed

The variations of flutter critical wind speed of the flat single-box deck model with wind yaw angle for various wind inclination angles are plotted in Fig. 13 using solid lines with dots. The curves of the critical wind speed of the model vs. wind yaw angle, estimated in the light of cosine rule based on the approach of mean wind decomposition and expressed with the following

equation, are also shown in the figure with dash-dot lines for comparison.

$$U_{cr}(\beta,\theta)=U_{cr}(0^{\circ},\theta)\big/\cos\beta \tag{2}$$

It can be seen from Fig. 13 that the flutter critical wind speed varies in an undulate manner with yaw angle, and the variation pattern largely depends on the inclination angle. The undulation of the critical flutter wind speed with the yaw angle becomes significant with the increase of the absolute value of the inclination angle. However, this kind of undulation is not significant at the inclination angle of 0°. This is because at the inclination angle of 0°, the shape of the flat single-box deck relative to the wind direction is quite close to a flat plate, and its aeroelastic performances of the oblique cross-sections along yaw winds should be very similar to that of the true cross section along the normal wind. Therefore, the cosine rule is approximately applicable in this case.

Nevertheless, with the increase of inclination angle, the shape of the flat single-box deck relative to the wind direction becomes bluffer and significantly different from a flat plate. Therefore, in the cases of non-zero inclination angles, the aeroelastic performance of oblique cross section will vary with the yaw angle and the cosine rule will inevitably lose its validity.

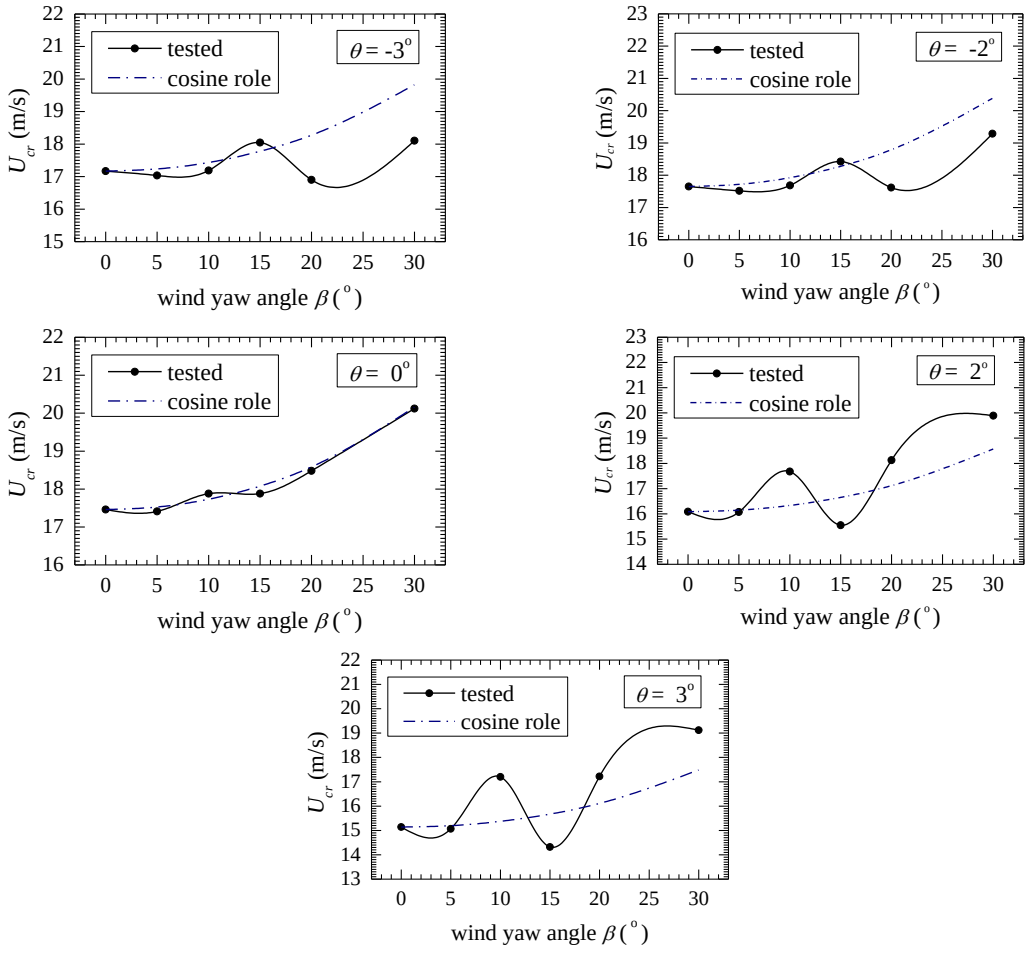

Fig.13 Critical wind speed of the flat single-box deck model vs. wind yaw angle

Table 2 lists the influence ratios of yaw wind effect on the flutter critical wind speeds of the flat single-box deck at various wind inclination angles, and Fig. 14 shows the corresponding curves of the influence ratios vs. yaw wind angle, where the influence ratio is defined as follows

$$IR_{cr}(\beta,\theta)=\left[U_{cr}(\beta,\theta)-U_{cr}(0^{o},\theta)\right]/U_{cr}(0^{o},\theta) \tag{3}$$

Table 2 Influence ratios of yaw wind effect (IR_{cr}) on U_{cr} of flat single-box deck (%)

β \ θ	-3°	-2°	0°	2°	3°
0°	0.0	0.0	0.0	0.0	0.0
5°	-0.8	**-0.8**	**-0.3**	-0.1	-0.5
10°	0.1	0.2	2.4	9.9	13.6
15°	5.1	4.4	2.4	**-3.3**	**-5.4**
20°	-1.6	-0.2	5.8	12.7	13.7
22.4°	**-2.9**	–	–	–	–
30°	5.4	9.3	15.2	23.7	26.3

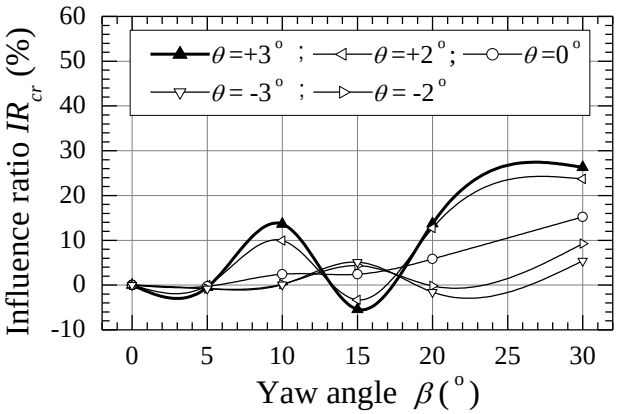

Fig. 14 Influence ratios of yaw wind effect (IR_{cr}) on U_{cr} of flat single-box deck vs. yaw angle

From Table 2 and Fig. 14, one can find that the lowest critical wind speed occur at a yaw angle between 5° and 25° for a certain inclination angle within the range from -3° to 3°, which is a common range of inclination angle for flutter checking specified in many guidelines for bridge wind-resistance design. The minimal critical wind speed occurs at the inclination angle 3° under the normal wind condition and at the yaw angle of 15° combined with the inclination angle of 3° under the skew wind condition. The yaw wind effect may decrease the minimal critical wind speed within a wind inclination angle range between -3° and 3° by about 6% for the flat single-box deck.

4.2 Flat π-shaped thin-wall deck

The structural damping ratio of the sectional model system of the flat π-shaped thin-wall deck at zero wind speed was also about 0.5%, and it was corrected to exact 0.5% when determining the flutter critical wind speeds based on the tested damping ratios of the model system. Fig. 15 shows the spline-fitted curves of the torsional vibration damping ratios of the flat π-shaped thin-wall deck model system vs. the test wind speed for different wind yaw angles and different model rotation angles. The corresponding flutter critical wind speeds can then be determined based on these curves of damping ratio using the same procedure mentioned in Section 4.1.

The variations of flutter critical wind speed of the flat π-shaped thin-wall deck with wind yaw angle for the various cases of wind inclination angles are plotted in Fig. 16 using solid lines with dots. The corresponding results, obtained using cosine rule as expressed by Eq. (2), are also plotted in Fig. 16 using dash-dot lines.

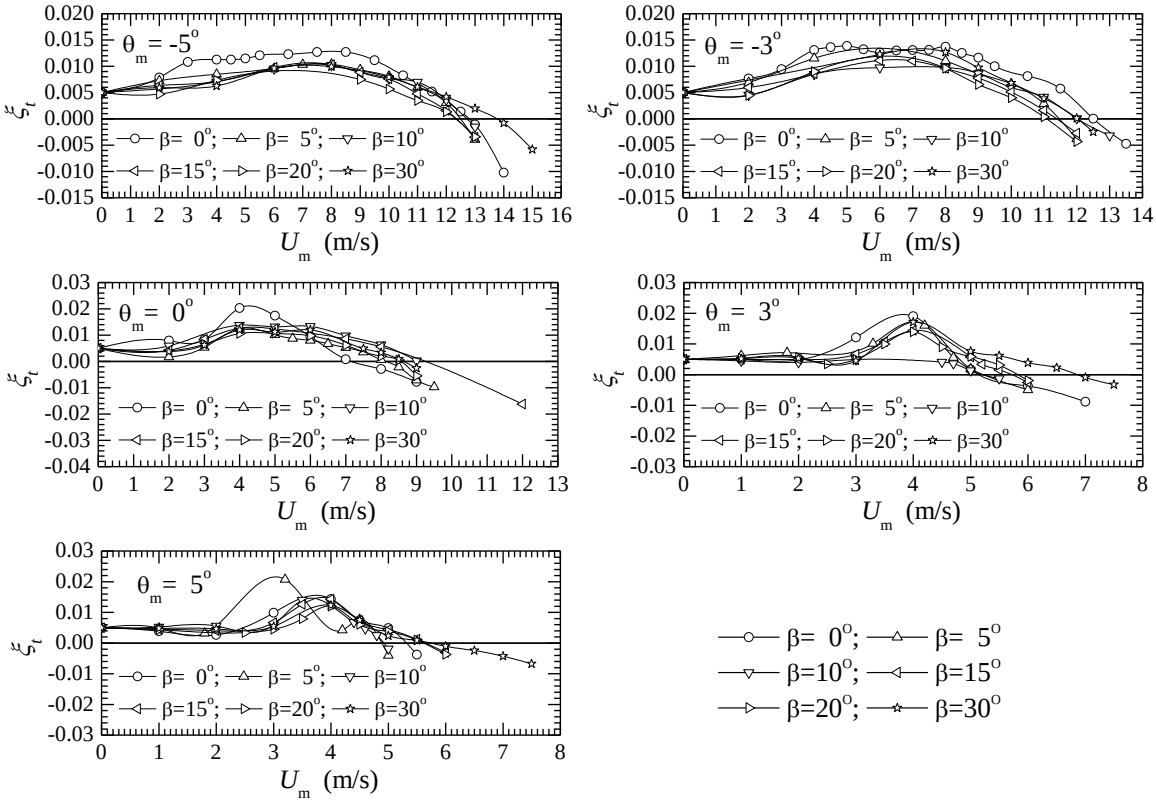

Fig. 15 Torsional vibration damping ratios of the flat π-shaped thin-wall deck model vs. wind speed

It can be found that the flutter critical wind speed of the flat π-shaped thin-wall deck also varies in an undulate pattern with the increase of wind yaw angle, and the variation pattern also largely depends on the inclination angle. Compared with the flat single-box deck, the inclination angle at which the cosine rule is approximately applicable moves from 0° to about 3°, and the undulation of flutter critical wind speed with yaw angle is much more significant for the negative inclination

angles than for the positive inclination angles.

The influence ratios of yaw wind effect on the flutter critical wind speed (IR_{cr}) of the flat π-shaped thin-wall deck at various wind inclination angles are shown in Table 3, and the corresponding variation curves of the influence ratio with the wind yaw angle are plotted in Fig. 17. It can be found that the lowest critical wind speed occurs at a yaw angle between 5° and 20° for the 3° inclination angle and the negative inclination angles between 0° and -3°, and happens at the 0° yaw angle (the normal wind case) for the 0° inclination angle and the positive inclination angles below 3°. Within the common inclination angle range from -3° to 3°, the minimal critical wind speed occurs at the inclination angle 3° under the normal wind condition, and at the yaw angle about 8.4° combined with the inclination angle of 3° under the skew wind condition. The yaw wind effect may drop the minimal critical wind speed within a wind inclination angle range between -3° and 3° by about 2% for the flat π-shaped thin-wall deck. However, for the inclination angles between -2° and -3°, the yaw wind effect may reduce the flutter critical wind speed of the flat π-shaped thin-wall deck by about 11%.

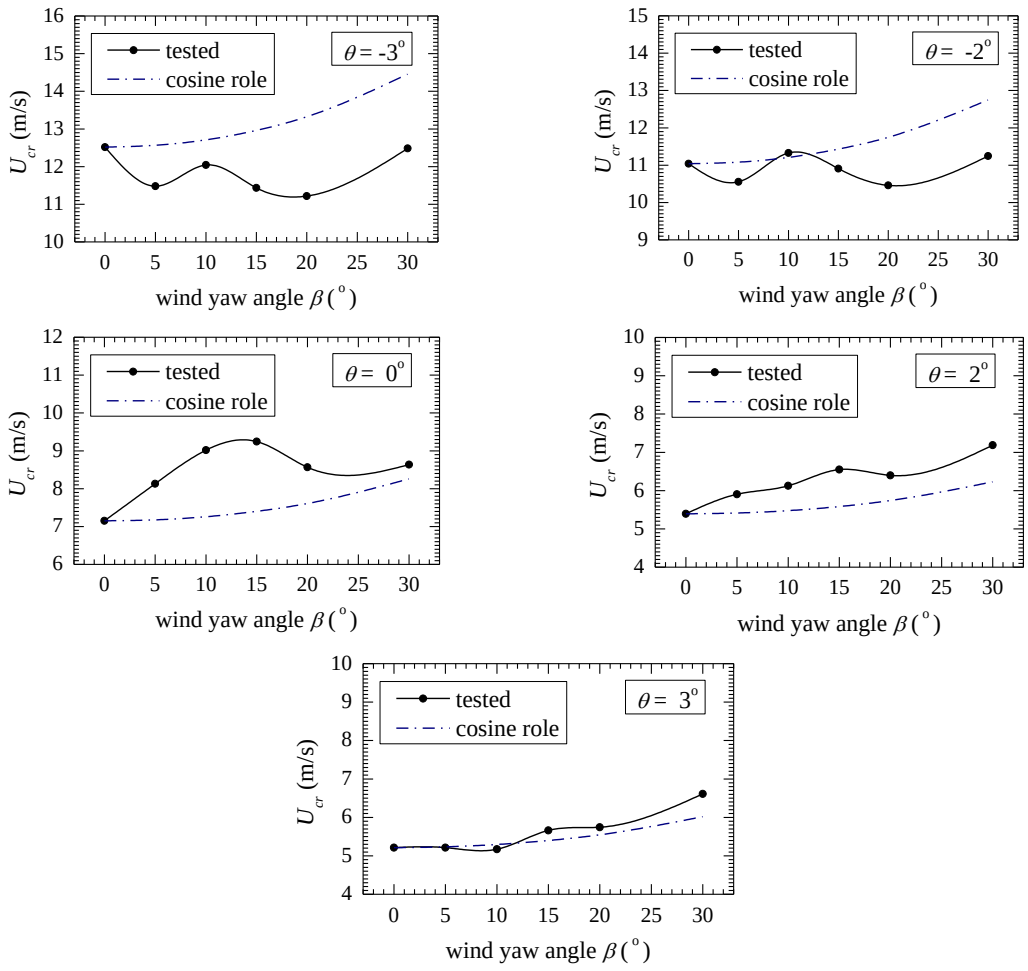

Fig. 16 Critical wind speed of flat π-shaped thin-wall deck model vs. wind yaw angle

Table 3 Influence ratios of yaw wind effect (IR_{cr}) on U_{cr} of flat π-shaped thin-wall deck (%)

β \ θ	-3°	-2°	0°	2°	3°
0°	0.0	0.0	**0.0**	0.0	0.0
5°	-8.3	-4.4	13.7	9.5	0.0
8.4°	–	–	–	–	**-1.5**
10°	-3.8	2.6	26.1	13.6	-0.8
15°	-8.6	-1.2	29.3	21.5	8.6
20°	**-10.4**	**-5.3**	19.8	18.7	10.2
30°	-0.3	1.9	20.8	33.3	26.8

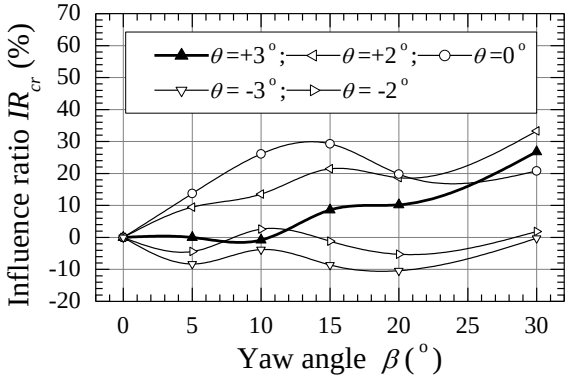

Fig. 17 Influence ratios of yaw wind effect (IR_{cr}) on U_{cr} of flat π-shaped thin-wall deck vs. yaw angle

4.3 Flat twin side-girder deck

Although the modal damping ratio of 2% is appropriate for a PC bridge, the structural damping ratio of the sectional model system of the flat twin side-girder deck at zero wind speed was adjusted to about 0.25% in this study so that the flutter phenomena could be observed in all testing cases. Later, the structural damping ratios of the sectional model system were exactly corrected to 0.25% when determining the flutter critical wind speeds based on the testing data of damping ratios of the model system.

Fig. 18 shows the spline-fitted curves of the torsional vibration damping ratios of the flat twin side-girder deck model system vs. the test wind speed for different wind yaw angles and different model rotational angles. The damping ratios were not identified for the test wind speed between 2-4 m/s because of the existence of significant vortex-induced vibrations, but this would not affect the determination of the flutter critical wind speed. The corresponding flutter critical wind speeds were then determined based on these damping curves using the same procedure mentioned in Section 4.1.

The solid lines with dots in Fig.19 show the variations of flutter critical wind speed of the flat twin side-girder deck with wind yaw angle for various cases of wind inclination angles, whilst the dash-dot lines represent the corresponding results obtained by using cosine rule expressed by Eq.

(2). It can be seen from Fig. 19 that the flutter critical wind speed of the flat twin side-girder deck also varies in an undulate pattern with the increase of wind yaw angle, and the variation pattern also largely depends on the inclination angle. Different from both the flat single-box deck and the flat π-shaped thin-wall deck, the undulation of flutter critical wind speed with yaw angle is much more significant for the positive inclination angles than for the negative inclination angles. The inclination angle at which the cosine rule is approximately applicable moves to about -2° for this type of bridge deck, but the discrepancy degree of the cosine rule result in this special case is slightly larger than that of the flat single-box deck and the flat π-shaped thin-wall deck.

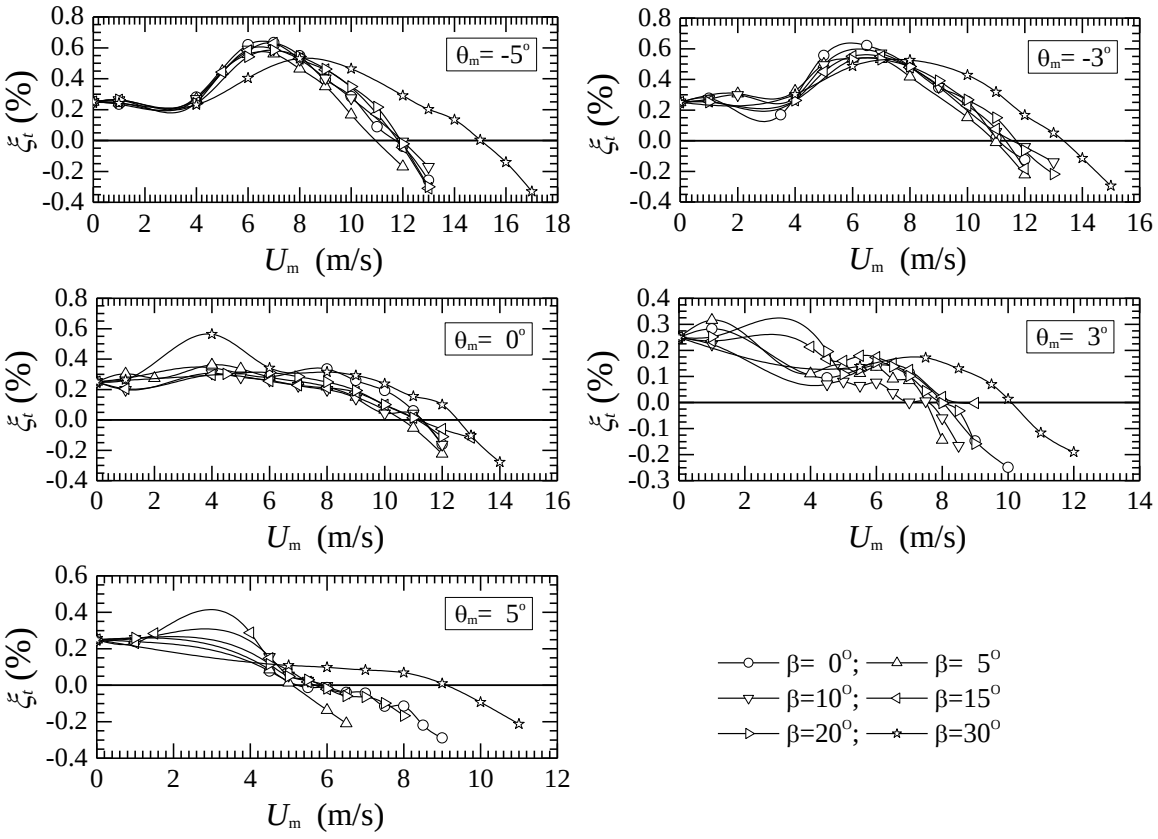

Fig. 18 Torsional vibration damping ratios of the flat twin side-girder deck model vs. wind speed

The influence ratios of yaw wind effect on the flutter critical wind speed of the flat twin side-girder deck at various inclination angles are shown in Table 4, and the corresponding variation curves of the influence ratio with the wind yaw angle are displayed in Fig. 20. One can find that the lowest critical wind speed occurs at a yaw angle between 5° and 10° for the inclination angles between -3° and 3°. Within the common inclination angle range from -3° to 3°, the minimal critical wind speed occurs at the inclination angle 3° under the normal wind condition, and at the yaw angle about 7.6° combined with the inclination angle of 3° under the skew wind condition.

The yaw wind effect may decrease the minimal critical wind within a wind inclination angle

range from -3° to 3° by about 8% for the flat twin side-girder deck.

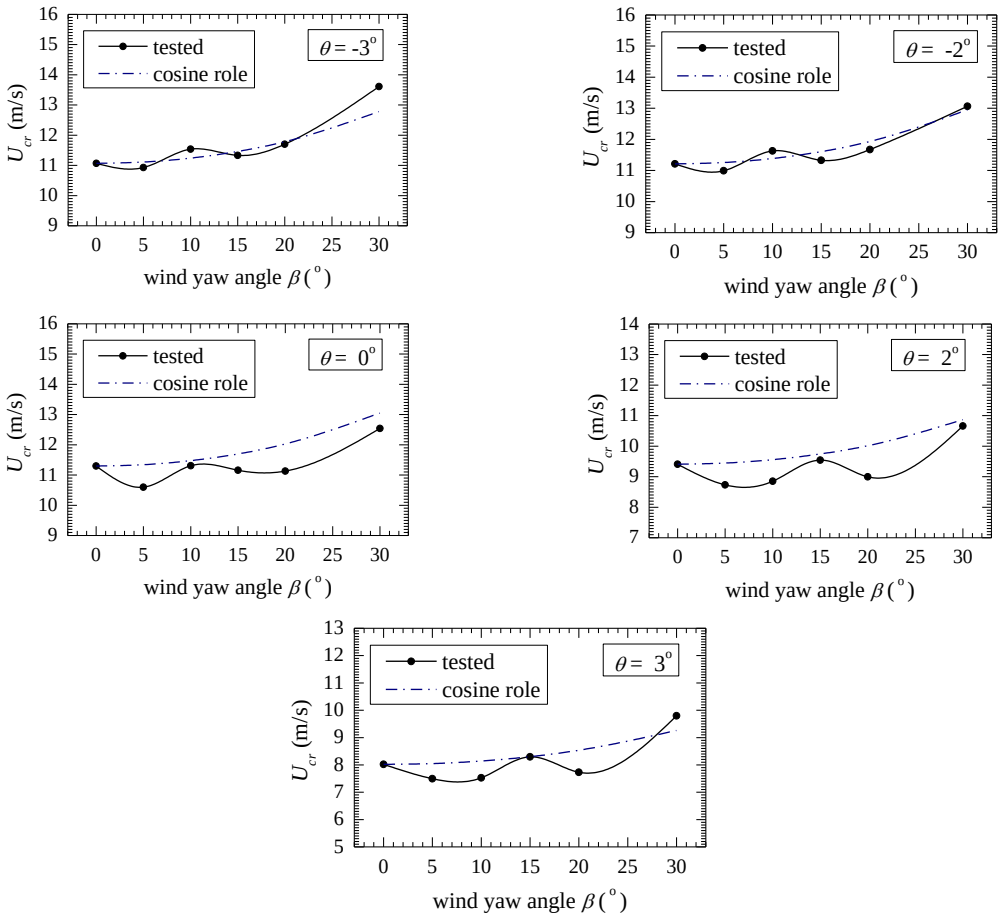

Fig. 19 Critical wind speed of flat twin side-girder deck model vs. wind yaw angle

Table 4 Influence ratios of yaw wind effect (IR_{cr}) on U_{cr} of flat twin side-girder deck (%)

β \ θ	-3°	-2°	0°	2°	3°
0°	0.0	0.0	0.0	0.0	0.0
5°	**-1.3**	**-2.0**	**-6.2**	-7.2	-6.5
7°	—	—	—	**-8.1**	—
7.6°	—	—	—	—	**-8.0**
10°	4.2	3.7	0.1	-5.9	-6.2
15°	2.4	1.0	-1.2	1.4	3.4
20°	5.7	4.1	-1.5	-4.4	-3.6
30°	22.9	16.5	11.0	13.3	22.2

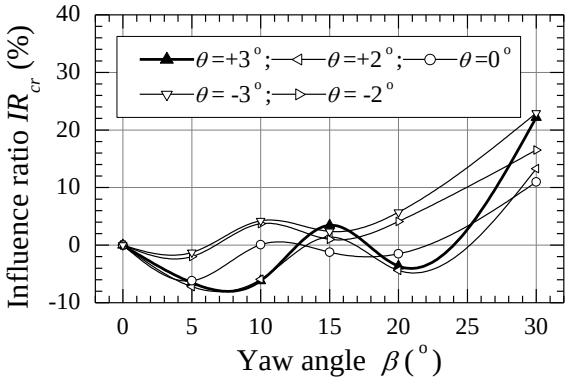

Fig. 20 Influence ratios of yaw wind effect (IR_{cr}) on U_{cr} of flat twin side-girder deck vs. yaw angle

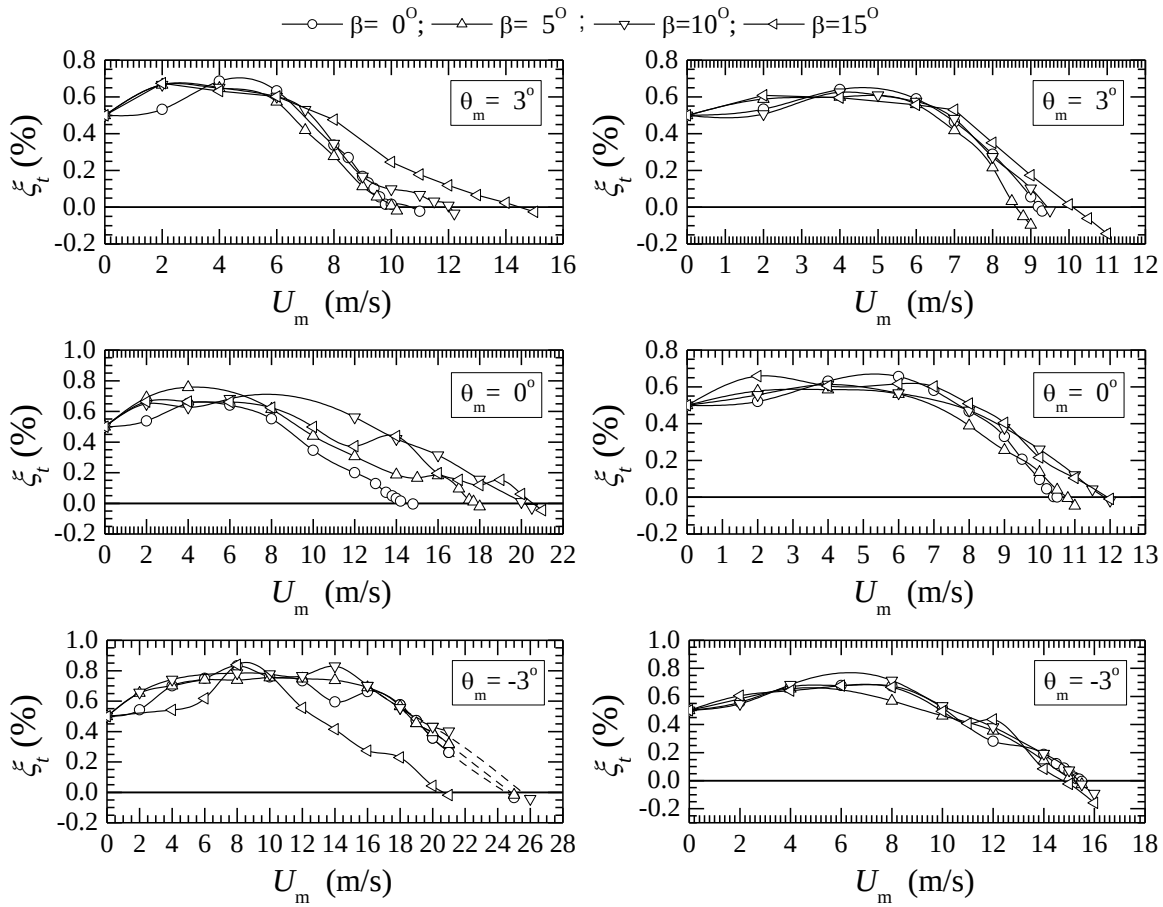

(a) with a central gap of 0.6m (b) without central gap

Fig. 21 Torsional vibration damping ratios of the truss-stiffened deck model vs. wind speed

4.4 Truss-stiffened deck

Two structural configurations of the truss-stiffened deck were tested in this study. One is the original configuration with a 0.6 m-wide gap at the center of the deck, and another is without the central gap by simply sealing the original gap in the test. The structural damping ratios of the sectional model system of the truss-stiffened deck at zero wind speed were also adjusted to about 0.5% for all testing cases, and were exactly corrected to 0.5% when determining the flutter critical wind speeds based on the testing data of damping ratios of the model system.

Fig. 21 shows the spline-fitted curves of the torsional vibration damping ratios of the truss-stiffened deck model system vs. the test wind speed for different wind yaw angles and different model rotation angles. The corresponding flutter critical wind speeds determined using the same procedure as mentioned in Section 4.1 are plotted in Fig. 22 as functions of the wind yaw angle for various cases of wind inclination angles. Fig. 22(a) is corresponding to the configuration with the central gap whilst Fig. 22(b) is for the configuration without the central gap. The dash-dot lines in these two figures represent the corresponding results obtained using cosine rule expressed by Eq. (2). The influence ratios of yaw wind effect on the flutter critical wind speed of the truss-stiffened deck at various inclination angles are shown in Table 5, and the corresponding variation curves of the influence ratio with the wind yaw angle are displayed in Fig. 23 for both configurations.

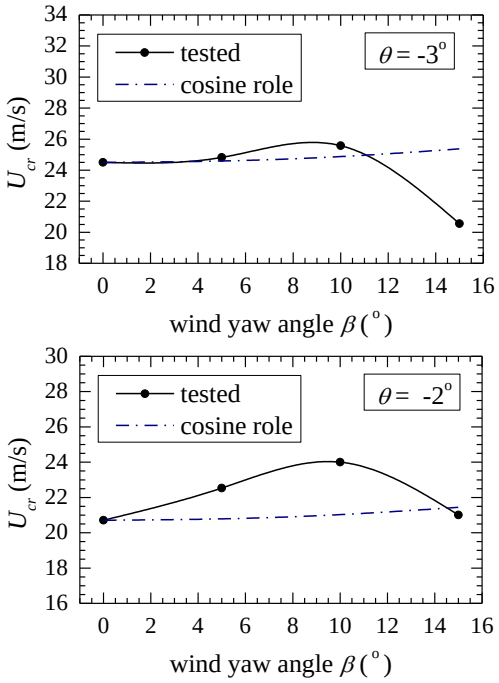

(a) with a central gap of 0.6m

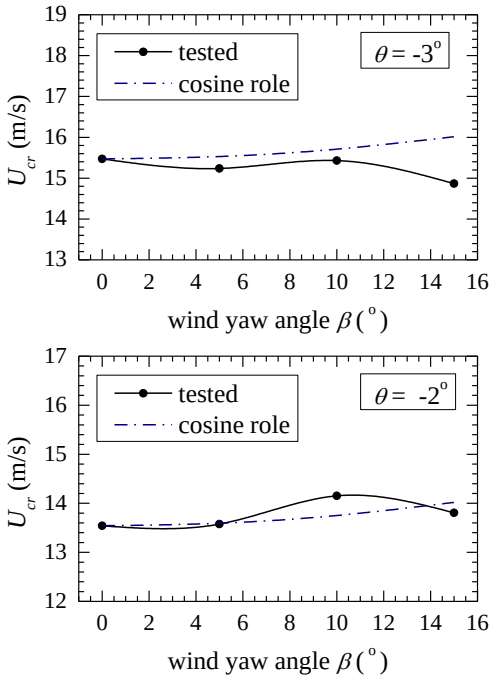

(b) without central gap

Continued

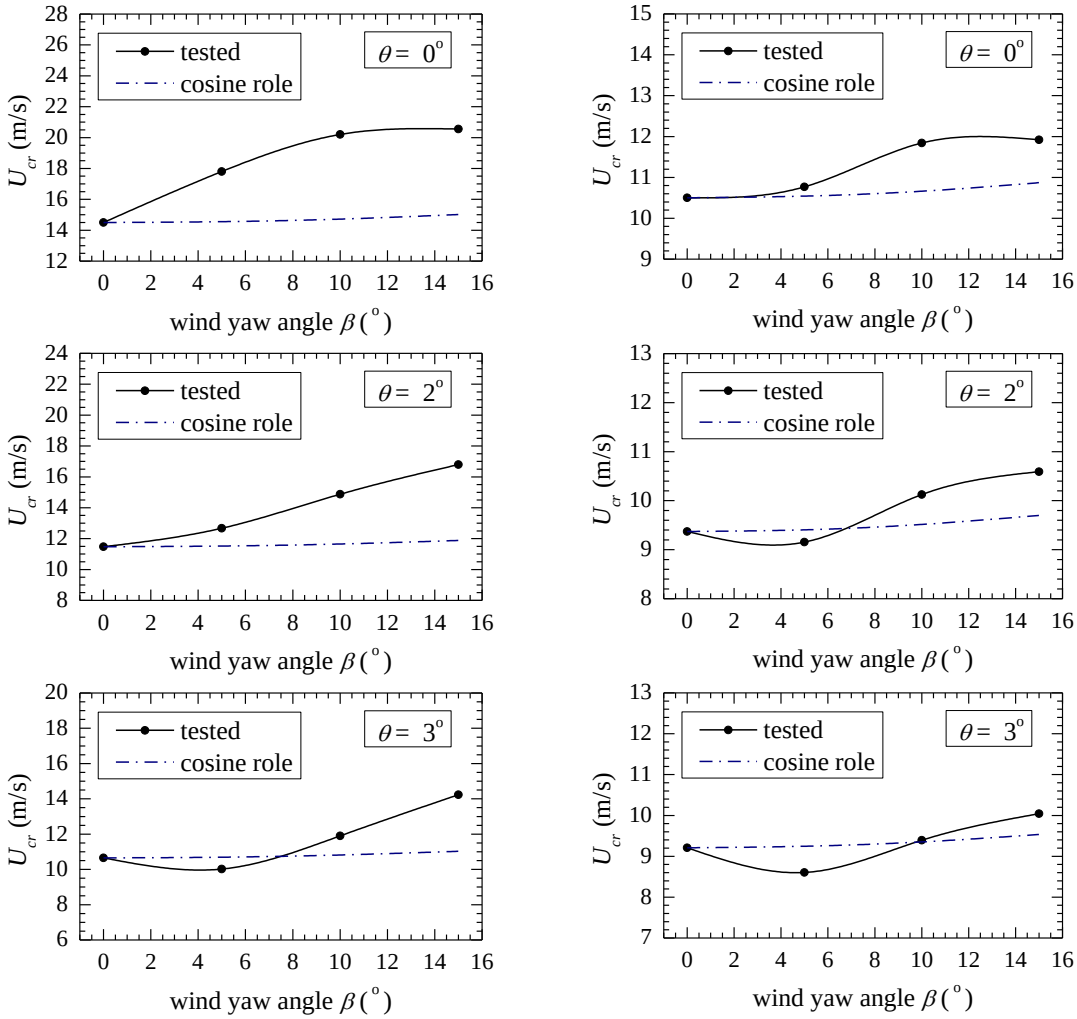

(a) with a central gap of 0.6m (b) without central gap

Fig. 22 (cont.) Critical wind speed of truss-stiffened deck model vs. wind yaw angle

Table 5 Influence ratios of yaw wind effect (IR_{cr}) on U_{cr} of truss-stiffened deck (%)

Configuration	With central gap					Without central gap				
β \ θ	-3°	-2°	0°	2°	3°	-3°	-2°	0°	2°	3°
0°	0.0	0.0	0.0	0.0	0.0	0.0	0.0	0.0	0.0	0.0
3.6°	–	–	–	–	–	–	–	–	**-3.0**	–
4°	–	–	–	–	**-6.4**	–	–	–	–	–
4.6°	–	–	–	–	–	–	–	–	–	**-6.6**
5°	1.3	8.8	22.8	10.4	**-5.9**	-1.5	0.3	2.6	-2.3	-6.6
10°	4.4	15.9	39.3	29.6	11.7	-0.3	4.5	12.8	8.1	2.0
15°	**-16.1**	1.4	41.7	46.4	33.7	**-3.9**	2.0	13.5	13.0	9.0

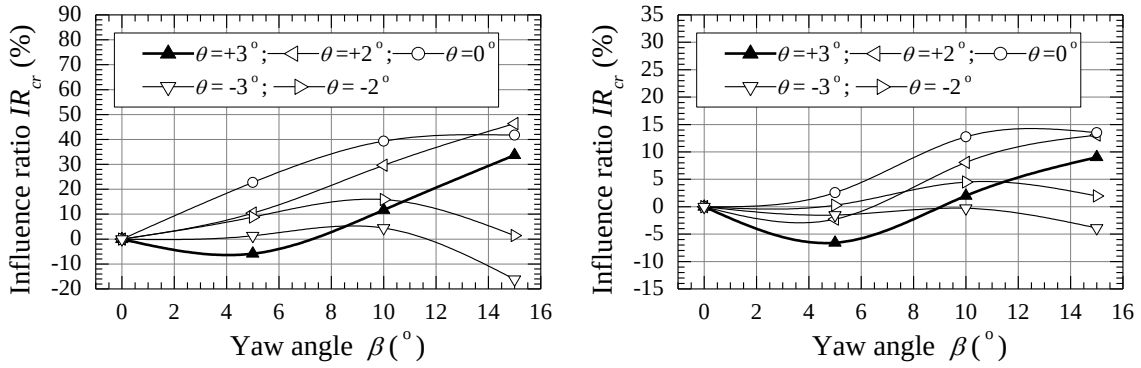

(a) with a central gap of 0.6m (b) without central gap

Fig. 23 Influence ratios of yaw wind effect (IR_{cr}) on U_{cr} of truss-stiffen deck vs. yaw angle

From Fig. 22 one can see that the discrepancies between the two sets of yaw wind-induced flutter critical wind speeds, obtained through the oblique sectional model tests and estimated by cosine rule, are significant for both configurations with and without the central gap. This means that the cosine rule is generally inappropriate for estimating the yaw wind flutter critical wind speed of truss-stiffened bridge decks. Furthermore, it can also be found that the variations of the flutter wind speed with the yaw angle are generally not monotonous for most cases of the wind inclination angle, and the variation pattern varies remarkably with the change of the wind inclination angle.

For the truss-stiffened deck with a 0.6m-wide central gap, one can see from Figs. 22(a), 23(a) and Table 5 that the minimal flutter critical wind speeds within the range of wind inclination angle between -3° and 3° always occur at the inclination angle of 3° for all the yaw wind angles from 0° to 15°. At the 3° inclination angle, the flutter critical wind speed reaches a minimum at a yaw angle of about 4°, which is about 6.4% lower than that under the normal wind condition. For the inclination angles between 0° and 2°, the flutter critical wind speed increases with the yaw angle up to 15°, but the increasing rate drops with the increasing wind yaw angle. For the negative inclination angles, the flutter critical wind speed increases first with the yaw angle up to 8-11°, and drops thereafter with the further increase of yaw angle up to 15°, and the peak yaw angle decreases with the increase of the absolute value of inclination angle. The lowest critical wind speed at the - 3° inclination angle occurs at yaw angle of 15° yaw and it is about 16.1% lower than that in the normal wind case.

For the truss-stiffened deck without the central gap, it can be seen from Figs. 22(b), 23(b) and Table 5 that the minimal flutter critical wind speeds within the range of wind inclination angle between -3° and 3° also occur at the inclination angle of 3° for all the yaw wind angles from 0° to 15°. At the 3° inclination angle, the variation pattern of the flutter critical wind speed with yaw angle is similar to that of the configuration with the central gap, and the flutter critical wind speed reaches a minimal value at a yaw angle of about 4.6°, which is about 6.6% lower than that under the normal wind condition. The variation pattern of the flutter critical wind speed with yaw angle at the 2° inclination angle is similar to that at the 3° inclination angle, and the lowest flutter critical

wind speed occurs at a yaw angle of about 3.6° and is about 3% lower than that under the normal wind condition. For the inclination angles between 0° and -2°, the flutter critical wind speed changes slightly when the yaw angle is less than 4-5°, and increases then with the yaw angle rising up to 13-10°, and drops thereafter with the further increase of yaw angle. The peak yaw angle also decreases with the increase of the absolute value of inclination angle. At the -3° inclination angle, the variation pattern of the flutter critical wind speed with yaw angle is clearly different from that of the configuration with the central gap. The flutter critical wind speed descends slightly first with the wind yaw angle increasing from 0° to 5°, and then it rises slightly within the yaw angle up to 10°. Afterwards, it drops again with the increasing wind yaw angle. The lowest flutter wind speed in the case of the -3° inclination angle occurs at a yaw angle of 15°, which is only about 3.9% lower than that in the normal wind case.

Furthermore, it can be seen that sealing the central gap can evidently reduce the flutter critical wind speeds of the truss-stiffened deck. However, it can notably diminish the undulation extent of the critical wind speed with the wind yaw angle on the other hand.

4.5 Variation of reynolds number with wind yaw angle

The Reynolds number used in the wind tunnel tests within the concerned range of wind yaw angle are listed in Table 6 for the five structure cases and three inclination angles (3°,0°,3°). The Reynolds number is calculated with reference of the width of the oblique cross section and the flutter critical wind speeds. It can be seen from Table 6 that the Reynolds number ranges from 1.6×10^5 to 8.3×10^5 for all test cases and varies with the wind yaw angle insignificantly with a maximal extent of 2.1×10^5. Therefore, the effect of the Reynolds number on the flutter critical wind speed is expected to be insignificant.

Table 6 Reynolds number ranges with the wind yaw angle

Structure case	**θ=3°**	**θ=0°**	**θ=-3°**
flat single-box deck	$4.1\text{-}6.2\times10^5$	$4.8\text{-}6.3\times10^5$	$4.6\text{-}5.9\times10^5$
flat π-shaped thin-wall deck	$1.6\text{-}2.4\times10^5$	$2.2\text{-}3.6\times10^5$	$3.8\text{-}4.4\times10^5$
Flat twin side-girder deck	$1.7\text{-}2.7\times10^5$	$2.4\text{-}3.3\times10^5$	$2.5\text{-}3.5\times10^5$
truss deck with gap	$3.2\text{-}4.8\times10^5$	$5.6\text{-}6.8\times10^5$	$6.9\text{-}8.3\times10^5$
truss deck without gap	$2.8\text{-}3.4\times10^5$	$3.3\text{-}4.0\times10^5$	$4.9\text{-}5.0\times10^5$

5. Preliminary discussion on the mechanism of yaw wind effect

The unfavorable effects of yaw wind on the flutter instability of four typical types of bridge decks were revealed via a series of wind tunnel tests of oblique sectional models. The unfavorable effects may lead to the reduction of the aeroelastic performance of an oblique cross-section along yaw wind compared with that of the true cross-section along the normal wind.

It is believed that when wind deviates from the normal direction, the hindrance and guidance of the deck front surface will lead to a span-wise flow, which may lower the aeroelastic performance of the oblique cross-section. In this connection, the flatter the deck is, the less the reduction on the aeroelastic performance. That is why the critical wind speed under yaw wind cases estimated by cosine rule agrees with the measured results quite well for the flat single-box deck at the inclination angle of zero. As an extreme case, if a flat plate is ideal with almost zero height, its aeroelastic performance of any oblique cross-section along yaw wind was the same as that of the normal one, and the cosine rule would perfectly work in this case. However, when the absolute value of inclination angle increases the bridge deck, even the ideal flat plate, becomes much bluffer, and besides its front surface, its upper or lower surface also exerts a significant hindrance and guidance effect on the flow. Consequently, the span-wise flow becomes stronger and stronger, and more and more complicated, leading to the more significant discrepancy between the results of flutter critical wind speeds obtained by the cosine rule and the test.

For the open cross-sections, such as the other three types of decks discussed in this paper, besides the reason above-mentioned the disturbance of the exposed transverse beams or transverse trusses on the wind flow should be an additional reason for the unfavorable effect of yaw wind on the flutter critical wind speed. Obviously, this kind of disturbance should be small at the normal wind case because the wind flow is parallel to the transverse beam or the transverse trusses. However, it will become significant when the wind deviates from the normal, and the enhancing rate of the disturbance may be very large at the initial stage of the yaw angle increase from 0°.

On the other hand, the normal component of wind speed decreases with the increase of wind yaw angle. It is still believed to be a positive effect on the flutter wind speed in the yaw wind cases, whilst the aeroelastic performance reduction mentioned before plays a negative effect. Synthetically, the flutter critical wind speed will decrease when the negative effect exceeds over the positive effect, and vice versa.

Furthermore, it is well known that with the increase of wind speed, the bridge torsional damping ratio increases generally first until a maximal value and then decreases towards negative, which corresponds to divergent vibration. Therefore, the rising phase length, the peak value and the dropping rate of damping ratio curves are three major factors to determine the flutter critical wind speed at the zero-damping ratio. By comparing the variation patterns of damping ratio with wind speed at different wind yaw angles as shown in Figs.12, 15, 18 and 21, one can find that the effect of wind yaw angle on the flutter critical wind speed is mainly attained via changing the rising phase length and the dropping rate of the damping ratio curves for the typical bridge decks concerned in this study. It can be further found that the most important factor causing the unfavorable effect of wind yaw angle on the flutter wind speed is the shrinkage of the rising phase of the damping ratio curves for the flat single-box deck, and it is the enhancement of the dropping rate of the damping ratio curves for the flat π-shaped thin-wall deck, the flat twin side-girder deck and the truss-stiffened decks. However, the influence of the wind yaw angle on the pattern of the damping ratio curves has no clear regularity because the disturbance of the deck body on the passing flow is extremely complicated under the yaw wind condition, resulting in the undulation phenomenon of the flutter critical wind speed with wind yaw angle.

The exact mechanism behind the unfavorable effect of the yaw wind on the flutter instability as well as the undulation manner of the flutter critical wind speed variation with yaw wind angle are not fully understood, except for the above preliminary understandings. This needs to be carefully investigated in the next step by exploring the affecting manners of wind yaw angle on the self-excited forces through direct force measurements in wind tunnels and on the 3D-flow pattern

around the bridge decks by means of 3D PIV or 3D CFD techniques, which are not mature yet at present.

6. Conclusions

The flutter instabilities of four typical bridge decks under skew winds were investigated via wind tunnel tests of oblique sectional models and discussed in this paper. The following concluding remarks can be drawn from this study:

(1) The wind direction normal to the bridge span is not absolutely the most unfavourable direction for the flutter instability of the four types of bridge decks tested. In fact, the lowest flutter critical wind speed often occurs in yaw wind case with a certain yaw angle between 5° and 20°.

(2) The flutter critical wind speed of bridge decks under skew wind varies with the wind yaw angle in an undulate manner generally. The variation pattern depends on the deck type and varies significantly with the change of wind inclination angle. For the three types of non truss-stiffened decks, the undulation of flutter critical wind speed with wind yaw angle becomes violent with the increase of the absolute inclination angle. For the flat single-box deck, the undulation extents are similar at the positive and negative inclination angles. However, for the flat π-shaped thin-wall deck the undulation is much more significant at the negative inclination angles than at the positive inclination angles, and the situation is reversed for the flat twin side-girder deck. For the truss-stiffened deck, the undulation extents are large at all inclination angles concerned when there is a narrow central gap on the bridge deck, but becomes obviously small when the central gap is sealed.

(3) For a certain wind inclination angle between -3° and 3°, the drop of critical wind speed due to the yaw wind effect may reach notable 6% for the flat closed single-box deck, 11% for the flat π-shaped thin-wall deck, 8% for the flat twin side-girder deck, 16% for the truss-stiffened deck with a narrow central gap, and 7% for the truss-stiffened deck without any gap, respectively.

(4) The yaw wind effect may reduce the minimal critical wind speed within the range of win inclination angle between -3° and 3°, which occurs at the 3° inclination angle for the bridge decks in this study, by about 6%, 2% and 8% respectively, for the flat closed single-box deck, the flat π-shaped thin-wall deck, the flat twin side-girder deck, and by about 7% for both the truss-stiffened decks with and without a narrow central gap. Therefore, the unfavorable effect of yaw wind on the flutter instability of long-span bridges should be considered seriously in the future practice, especially for the supper-long span bridges in strong wind regions, for which only small redundancy on the flutter critical wind speed can be attained in most cases.

(5) The cosine rule based on the mean wind decomposition is generally inapplicable for the estimation of the flutter critical wind speed of long-span bridges under skew winds, at least for the four typical types of bridge decks discussed in this paper.

Acknowledgments

The work described in this paper was jointly supported by the Fundamental Research Fund for State Key Laboratories of China (Grant No. SLDRCE08-A-02), the National Nature Science Foundation of China (Grant 50978204, 91215302), and the Hong Kong Research Grants Council (PolyU5304/11E), to which the writers are most grateful. Any opinions and concluding remarks presented here are entirely those of the writers.

References

Agar, T.J.A. (1989), "Aerodynamic flutter analysis of suspension bridges by a modal technique", *Eng. Struct.*, **11**(2), 75-82.

Bietry, J., Delaunay, D. and Conti, E. (1994), "Comparison of full-scale measurement and computation of wind effects on a cable-stayed bridge", *Proceedings of the International Conference A.I.P.C.-F.I.P.*: *Cable-stayed and Suspension Bridges*, Deauville, France, 12-15 Oct.

Chen, X. (2007), "Improved understanding of bimodal coupled bridge flutter based on closed-form solutions", *J. Struct. Eng.- ASCE*, **133**(1), 22-31.

Ding, Q.S., Chen, A.R. and Xiang, H.F. (2002), "Coupled flutter analysis of long-span bridges by multimode and full-order approaches", *J. Wind Eng. Ind. Aerod*., **90**(12-15), 1981-1993.

Ge, Y.J. and Tanaka, H. (2000), "Aerodynamic flutter analysis of cable-supported bridges by multi-mode and full-mode approaches", *J. Wind Eng. Ind. Aerod.*, **86**(2-3), 123-153.

Hua, X.G. and Chen, Z.Q. (2008), "Full-order and multimode flutter analysis using ANSYS", *Finite Elem. Anal. Des.*, **44**(9-10), 537-551.

Jain, A., Jones, N.P. and Scanlan, R.H. (1996), "Coupled flutter and buffeting analysis of long-span bridge", *J. Struct. Eng. - ASCE*, **122**(7), 716-725.

Katsuchi, H., Jones N.P., and Scanlan R.H. (1999), "Multimode coupled flutter and buffeting analysis of the Akashi-Kaikyo bridge", *J. Struct. Eng. - ASCE*, **125**(1), 60-70.

Kimura, K. and Ohara, T. (1999), "Lateral sway buffeting of bridge decks due to yawed wind", *Proceedings of the 10th International Conference on Wind Engineering: Wind Engineering into 21st Century*, Copenhagen, Denmark, 21-24, June**.**

Kimura, K. and Tanaka, H. (1992), "Bridge buffeting due to wind with yaw angles", *J. Wind Eng. Ind. Aerod.*, **41-44,** 1309-1320.

Kimura, K., Nakamura, S. and Tanaka, H. (1994), "Buffeting analysis for cable-stayed bridges during construction in yawed wind", *Proceedings of the International Conference A.I.P.C.-F.I.P.*: *Cable-stayed and Suspension Bridges*, Deauville, France, 12-15 Oct.

Kirch, Arno and Peil, Udo (2012), "Limitations for the control of wind-loaded slender bridges with movable flaps", *Wind Struct.*, **15**(5), 441-462.

Mishra S.S., Kumarb K. and Krishna P. (2008), "Multimode flutter of long-span cable-stayed bridge based on 18 experimental aeroelastic derivatives", *J. Wind Eng. Ind. Aerod.*, **96**(1), 83-102.

Mishra S.S., Kumarb K., Krishna P. (2008), "Relevance of eighteen flutter derivatives in wind response of a long-span cable-stayed bridge", *J. Struct. Eng. - ASCE*, **134**(5), 769-781.

Namini, A., Albrecht, P. and Bosch, H. (1992), "Finite element-based flutter analysis of cable-suspended bridges", *J.. Struct. Eng. - ASCE*, **118,** 1509-1526.

Ø iseth, O., Rönnquist, A. and Sigbjörnsson, R. (2011), "Time domain modeling of self-excited aerodynamic forces for cable-supported bridges: A comparative study", *Comput. Struct.*, **89**(13-14), 1306-1322.

Phan, D.H. and Kobayshi, H. (2011), "An experimental study of flutter and buffeting control of suspension bridge by mechanically driven flaps", *Wind Struct*., **14**(2), 153-165.

Scanlan, R.H. (1978), "The action of flexible bridge under wind, I: flutter theory", *J. Sound Vib.*, **60,** 187-199.

Scanlan, R.H. (1993), "Bridge buffeting by skew winds in erection stages", *J. Eng. Mech. - ASCE,* **119**(2), 251-269.

Scanlan, R.H. (1999), "Estimates of skew wind speeds for bridge flutter", *J. Bridge Eng.- ASCE,* **4,** 95-98.

Scanlan, R.H. and Gade, R.H.(1977), "Motion of suspension bridge spans under gusty wind", *J. Struct. Div. - ASCE,* **103**(9)**,** 1867-1883.

Strømmen, E. and Hjorth-Hasen, E. (1995), "The buffeting wind loading of the structural members at an arbitrary attitude in the flow", *J. Wind Eng. Ind. Aerod*., **56**(2-3), 267-290.

Xie, J. and Tanaka, H. (1991), "Buffeting analysis of long span bridges to turbulent wind with yaw angle", *J. Wind Eng. Ind. Aerod*., **37**(1)**,** 65-77.

Xu, Y.L. and Zhu, L.D. (2005), "Buffeting response of long-span cable-supported bridges under skew winds — part II: case study", *J. Sound Vib*., **281**(3-5)**,** 675-697.
Xu, Y.L., Zhu, L.D., Wong, K.Y. and Chan, K.W.Y. (2000), "Field measurement results of Tsing Ma suspension bridge during Typhoon Victor", *Struct. Eng. Mech.*, **10**(6)**,** 454-559.
Zahlten W. and Eusani R. (2006), "Numerical simulation of the aeroelastic response of bridge structures including instabilities", *J. Wind Eng. Ind. Aerod.*, **94**(11), 909-922.
Zhang, W.M., Ge, Y.J. and Levitan, M.L. (2011), "Aerodynamic flutter analysis of a new suspension bridge with double main spans", *Wind Struct.*, **14**(3), 187-208.
Zhang, X. (2007), "Influence of some factors on the aerodynamic behavior of long-span suspension bridges", *J. Wind Eng. Ind. Aerod.*, **95**(3), 149-164.
Zhang, X. and Brownjohn, J.M.W. (2005), "Some considerations on the effects of theP-derivatives on bridge deck flutter", *J. Sound Vib.*, **283**, 957-969.
Zhang, Z.T., Chen, Z.Q., ASCE, M., Hua, X.G., Li, C.G. and Ge, Y.J. (2010), "Investigation of turbulence effects on torsional divergence of long-span bridges by using dynamic finite-element method", *J. Bridge Eng. - ASCE*, **15**(6), 639-652.
Zhu, L.D. and Xu, Y.L. (2005), "Buffeting response of long-span cable-supported bridges under skew winds - part I: theory", *J. Sound Vib*., **281**(3-5), 647-673.
Zhu, L.D., Ren, P.J. and Chen, W. (2011), "Field measurement of wind profiles in the Balinghe deep gorge in South-west China", *Proceedings of the 13th International Conference on Wind Engineering*, Amsterdam, The Netherlands, 10-15 July (Electronic).
Zhu, L.D., Xu, Y.L. and Xiang, H.F. (2002b), "Tsing Ma bridge deck under skew winds - part II: flutter derivatives", *J. Wind Eng. Ind. Aerod.*, **90**(7), 807-837.
Zhu, L.D. and Xiang, H.F. (1995), "Mass-system simulation of sectional model for bridge flutter", *Structural Engineers*, **35**(4), 39-45. (in Chinese).
Zhu, L.D., Xu, Y.L., Zhang, F. and Xiang, H.F. (2002a), "Tsing Ma bridge deck under skew winds - part I: aerodynamic coefficients", *J. Wind Eng. Ind. Aerod.*, **90**(7), 781-805.

CC